Cosmic Masers: Proper Motion toward the Next-Generation Large Projects
Proceedings IAU Symposium No. 380, 2024
T. Hirota, H. Imai, K. Menten, & Y. Pihlström, eds.
doi:10.1017/S1743921323002399

Flaring Masers and Pumping

M. D. Gray[1], S. Etoka[2], B. Pimpanuwat[2], A. M. S. Richards[2] and F. J. Cowie[2]

[1]National Astronomical Research Institute of Thailand, 260 Moo 4, T. Donkaew, A. Maerim, Chiangmai 50180, Thailand. email: malcolm@narit.or.th

[2]Jodrell Bank Centre for Astrophysics, Department of Physics and Astronomy, University of Manchester, M13 9PL, UK.

Abstract. We briefly consider the history of maser variability, and of flaring variability specifically. We consider six proposed flare generation mechanisms, and model them computationally with codes that include saturation and 3-D structure (the last mechanism is modelled in 1-D). Fits to observational light curves have been made for some sources, and we suggest that a small number of observational parameters can diagnose the flare mechanism in many cases. The strongest flares arise from mechanisms that can increase the number density of inverted molecules in addition to by geometrical effects, and in events where unsaturated quiescent masers become saturated during the flare.

Keywords. masers, molecular processes, radiative transfer, radio lines: ISM

1. Introduction

A significant advance in the study of variability in astrophysical masers towards star-forming regions was the long-term, high-cadence, monitoring of 6.7-GHz methanol masers over more than 4 yr by Goedhart *et al.* (2004). The time resolution of 1–2 weeks for most sources was enough to show that the majority vary, and do so with a variety of patterns, including monotonic rise or fall, and aperiodic, quasi-periodic and periodic oscillations. Periods of the sources in the dataset in Goedhart *et al.* (2004) covered 132–520 d. Since then, there have been extensions to both longer (longest at time of writing 1260 d, Tanabe *et al.* 2023) and shorter (for example, 23.9 d, Sugiyama *et al.* 2017) periods, and other variability phenomena have been studied. These include variability correlations with other methanol maser transitions, such as 12.2 GHz (Goedhart *et al.* 2009), with transitions in other species, for example OH and H_2O (MacLeod *et al.* 2018), and with infra-red (IR) continuum radiation, likely involved in maser pumping (Moscadelli *et al.* 2017; Kobak *et al.* 2023). Anti-correlated behaviour between flares in 22-GHz H_2O and 6.7-GHz methanol masers, for example, Olech *et al.* (2020), suggests these transitions are pumped by different mechanisms. Although there is no accepted definition of flaring variability, it can perhaps be considered as a more than usually powerful change in the flux density of one or more spectral features. Periodicity, if found, links maser flares to astrophysical properties of the system, such as orbital parameters (Parfenov and Sobolev 2014; van der Walt *et al.* 2016) and stellar pulsation (Inayoshi *et al.* 2013). Useful analysis is very reliant on good flare monitoring data, such as that provided by the M2O organization† (Burns *et al.* 2022), and multi-band data that can identify IR or radio continuum correlations with the maser emission.

† www.masermonitoring.com/

The analysis in the present work relies on approximating the maser system as a series of time-independent snapshots. Therefore, events on timescales $< 1 - 5$ d, dependent on the mechanism, are beyond the scope of this model. In particular, we cannot address variability that requires fully time-dependent models of the sort required to model superradiance (Rajabi *et al.* 2019), pump fluctuations (Clegg and Cordes 1991), or other very short timescales (hours, minutes or less). Notwithstanding these limitations, we consider the variations in flare properties from the following mechanisms: (1) rotation of aspherical clouds, (2) variation in the energy density of pumping radiation, (3) variation in the intensity of the amplified background radiation, (4) shockwave impact on an initially spherical cloud, (5) cloud overlap in the line of sight, and (6) catastrophic release of saturation under the assumption of complete velocity redistribution (CVR: see Section 1.6).

1.1. *Rotating Clouds: Rotors*

Prolate and oblate rotors were considered by Gray *et al.* (2019) in a model that includes full saturation of the maser. The distortion algorithm applied ensured that the prolate and oblate objects preserved the volume of a 'parent' sphere. Average light-curves from many viewpoints show variability indices F/F_0 of typically a few to few tens, where F is the line-centre flux density at flare maximum and F_0 is the quiescent flux density in the same channel. Stability considerations make long-term periodicity and short flares, with a timescale shorter than the sound-crossing time of the cloud, very unlikely. In common with many mechanisms, saturation reduces the variability index, but if saturation is not achieved at the peak of the flare, the flaring object may not be bright enough to be observable. The duty cycle, the fraction of time that the light curve is above half its peak value is modest, typically in the range $0.1 - 0.3$.

1.2. *Variation in the Pumping Radiation*

In this mechanism, the pumping radiation follows a light curve that we shall call the 'driving function'. The light curve of the maser is then a distortion of the driving function, highly modified by amplification and saturation (see Figure 1). In most cases, the maser light curves emphasize the brighter parts of the driving function and suppress the weaker parts, so that the duty cycle of the maser light curve is the lower: almost always < 0.3 and typically ~ 0.1. The driving functions used range from a basic sinusoid to representations of stellar pulsation and periodic orbital effects based on accretion and colliding binary winds. Details are given in the caption of Figure 1. The highest variability indices from this mechanism can exceed 10^7, but to achieve such a value typically requires a very low optical depth in the quiescent cloud, and the maximum flux density in the flare is only modest. Some compromise is therefore required between the variability index and the maximum flux density achieved, noting that it is this latter parameter that controls the observability of the flare (Gray *et al.* 2020b). The ability of this mechanism to produce powerful flares arises as a natural consequence of generating more inverted molecules, rather than depending simply on geometry, though aspherical clouds were also considered in Gray *et al.* (2020b).

1.3. *Variation in the Background Radiation*

If the level of background radiation is sufficient to generate a saturated maser, then further increase in the background intensity does little to the output; only a significant fall in the background, that lifts saturation, produces a large effect on the maser (Gray *et al.* 2020b). The light curve from this mechanism is therefore characteristically different from what is typical of those from Section 1.2. A maser light curve driven by background

https://doi.org/10.1017/S1743921323002399 Published online by Cambridge University Press

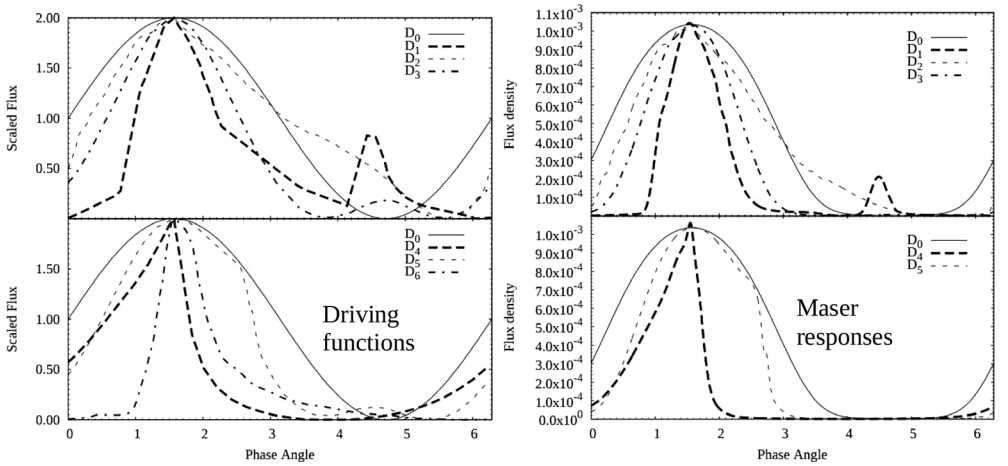

Figure 1. Sample periodic driving functions (left panel) and maser responses (right panel). The driving functions are, D_0: sinusoid, D_1: IR continuum digitized from Stecklum *et al.* (2018), D_2: theoretical Cepheid light curve from Bhardwaj *et al.* (2017), D_3–D_5: light curves for stars only, shock only, and combined effect by van der Walt *et al.* (2016) from the spiral shock model of Parfenov and Sobolev (2014), D_6: background radiation light curve from the colliding wind eccentric binary model by van der Walt *et al.* (2009). The responses were generated from models with a maser depth range of 5.0–10.0 between quiescent and flare peaks, and for a prolate cloud viewed along its long axis.

variability (driving function D_6) typically has a long duty cycle (> 0.5), increasing with saturation, as demonstrated in Figure 2 (left panel), though it shares with the variable pump a natural periodicity if the driving function is also periodic. The typical shape of the light curve with this mechanism, and strong saturation has been referred to as an 'anti-flare'. Candidate objects from Goedhart *et al.* (2004) include G338.92−0.06 and G351.78−0.54.

1.4. *Shock Compression*

The key to this mechanism is a compression of the gas and the establishment of lines of sight parallel to the shock front, and within the shocked material, that exhibit lengths comparable to the diameter of the original cloud, but contain significantly more material. A very rapid initial rise in the maser output, over the first 20–50 d, is followed by a slower rise as the shock progresses (Figure 2 upper right). Relaxation has been approximated as an exponential decay, based on the sound crossing time in the shocked material. Unlike the variable radiation mechanisms discussed above, shock-generated maser flares are therefore highly directional (Gray *et al.* in preparation) as shown in Figure 2, lower right graph. Chemical effects may also increase the actual number of inverted molecules within the cloud in the case of H_2O molecules (Kaufman and Neufeld 1996), and populations can also be increased by shock-induced release from grain surfaces, for example in Class 1 methanol masers (Sobolev 1993). The great structural change imposed by the shock makes periodicity impossible for a single cloud and the pattern of decay of the flare very difficult to predict, but a periodically generated shock wave could cause a quasi-periodic flare if it struck a number of similar clouds on each new passage. In the ideal isothermal hydrodynamic case, this mechanism provides the largest variability indices, of order 10^8, but values of 10^5 can still be achieved by more realistic MHD shocks.

https://doi.org/10.1017/S1743921323002399 Published online by Cambridge University Press

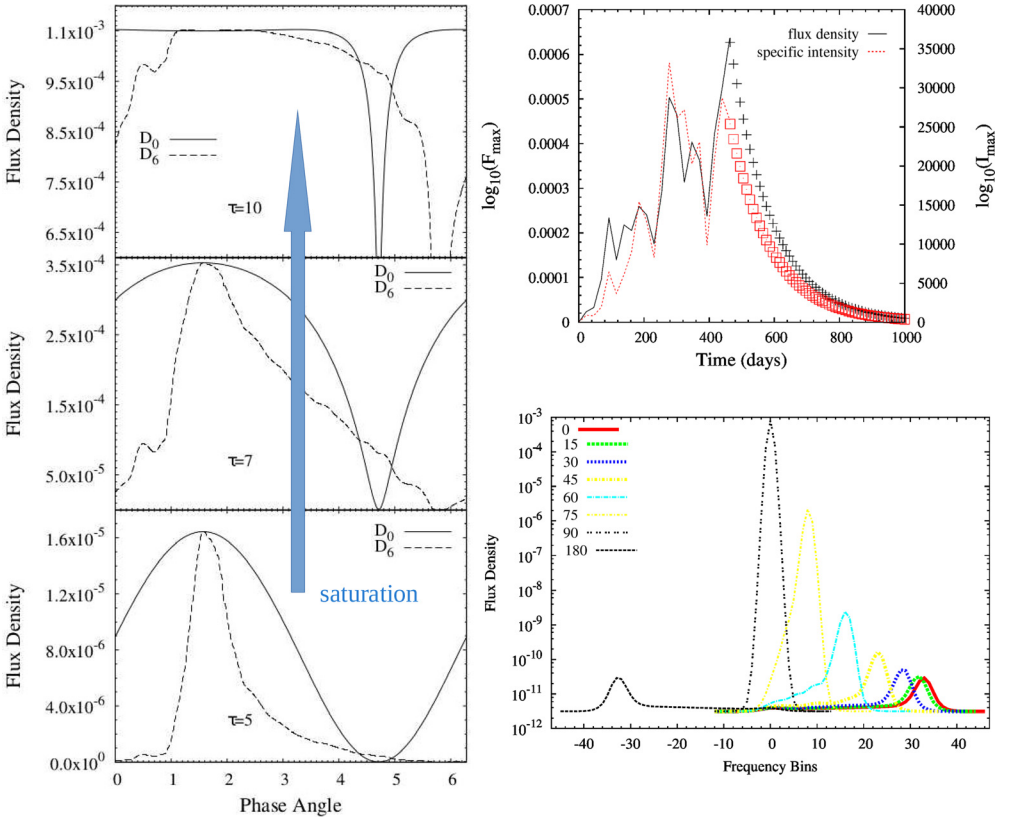

Figure 2. Left panel: periodic light curves for the variable background mechanism driven by the driving functions D_0 and D_6 (see Figure 1); the most saturated model is at the top. Upper right panel: the light curve generated by a hydrodynamic isothermal shock of speed $7.5\,\mathrm{km\,s^{-1}}$ striking an initially spherical cloud of radius 1 au containing 10.9 inverted ortho-H_2O molecules $\mathrm{cm^{-3}}$. Curves are shown for the flux density in the brightest spectral channel and the specific intensity in the brightest pixel (right-hand y-axis). Lower right panel: the effect of varying the viewing angle on the maser spectrum in the fully shocked cloud. Angles vary from 0°, facing the approaching shock, through 90°, parallel to the shock front to 180° (behind the shock). All the graphs in this figure use a specific intensity scaled to the saturation intensity. With a background level of 10^{-6} and an observer at a distance of 1000 domain units, the flux density then has a background level of $\pi \times 10^{-12}$.

1.5. *Line of Sight Overlap*

The idea of a continuous Keplerian disc as the source of varying masers in a star forming region goes at least as far back as the study of S255 by Cesaroni (1990). For discrete clouds, considerable preliminary work on discs has been carried out for a massive star-formation scenario (Cowie *et al.* in preparation). The duration of an overlap then depends on the viewing angle (ϕ, see Figure 3, top left). The effect of varying ϕ, and consequently the velocity-coherent gain path, is explored in Figure 3 (top right). Behaviour also strongly depends on the orbital radii. Two clouds with a small separation in orbital radius generate a flare of very long duration (thousands of days), but rise and decline on order of a year is typical of orbital radii of a few hundred au, with 100 au orbital spacing, orbiting a central object of $>10\,\mathrm{M_\odot}$. Light curves show considerable sub-structure if one, or both, clouds are aspherical and rotating with a rotation period similar to the duration of the overlap (Figure 3, bottom left). The variability index for overlaps appears limited

https://doi.org/10.1017/S1743921323002399 Published online by Cambridge University Press

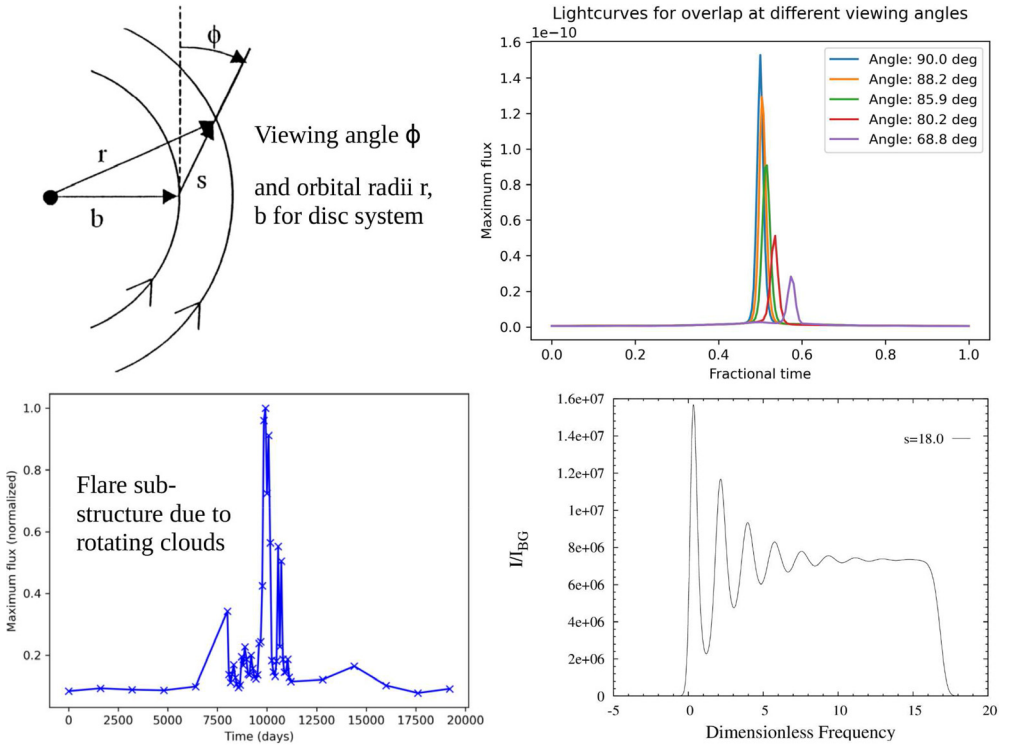

Figure 3. Top left: Angle and radius definitions for overlap in a disc system (Watson and Wyld 2000). Top right: Effect of viewing angle on overlap-based flare light curves. Bottom left: substructure in flare light curve due to rotating clouds: $r = 53$ au, $b = 50$ au, $\phi = 90°$. Flux density scale as in Figure 2, except that the observer is at 10000 domain units. Bottom right: Spectrum of a CVR catastrophe flare: intensity scaled to the background for a 1-D model is plotted against dimensionless frequency, scaled to the Doppler width, at a dimensionless distance, s, or velocity shift in Doppler units, of 18.0.

to $\lesssim$500, and is highest for a cloud pair with orbital radii of 1850 and 1300 au, and where the individual clouds are unsaturated, but the pair shows significant saturation. Much faster flares can of course be generated by random hyperbolic encounters. Periodicity is unlikely, but possible in a discrete-cloud disc system.

1.6. *Saturation Catastrophe*

This is a more subtle effect that requires a maser system with CVR, where transfer of population between the velocity subgroups of a quantum-mechanical energy level, that happens to be the upper or lower level of a maser transition, is maintained at a rate comparable to the maser pump rate. Such rapid redistribution operates through a network of optically thick IR transitions (Goldreich and Kwan 1974). Under CVR, the molecular response must saturate as a whole, and remains approximately Gaussian, even under very strong saturation. With a velocity gradient in the line of sight, a very strong maser line can maintain saturation even as the molecular response in the maser transition begins to shift away from the centre of the line. At a certain shift, the saturation is catastrophically released, and a new maser feature appears at the new, shifted line centre of the molecular response. A system can display several ‘echoes’ of this initial phenomenon, but the amplitude generally decreases for the second and subsequent maser peaks (see Figure 3, bottom right). The velocity spacing between peaks is not quite

https://doi.org/10.1017/S1743921323002399 Published online by Cambridge University Press

periodic. For the optimum parameter choices, the variability index on the initial maser peak can be as high as several million.

2. Fits to Data

At least for the mechanisms based on IR and background variability, just three observational parameters, namely the duty cycle, variability index and flux density at peak may be plotted as sets of contours on a diagram with axes showing two computational parameters, the maser optical depth under quiescent conditions, and the change in the maser optical depth (or the background intensity) during the flare (Gray *et al.* 2020b). In this way a fit can be found from the crossing places of the contours, leading to a fitted computational light curve. The flux density achieved is used to check for consistency between modelled and observed sizes of the maser objects, or 'clouds', noting that, owing to beaming, observed maser sizes can be considerably smaller than the objects from which the emission arises. This fitting technique has been applied to a spectral component of the flare in G107.298+5.65, and to two components of the flare in S255-NIRS3 with satisfactory results (Gray *et al.* 2020a). Source choice for the fitting procedure was strongly based on the availability of contemporaneous, high-cadence IR or continuum background data, which is vital for establishing a driving function.

It is likely that the maximum flux density and variability index can also be used as key observational parameters in the analysis of other mechanisms. However, in the absence of periodicity, the duty cycle requires replacement with a more general temporal parameter, such as the rise time of the flare or the asymmetry, between rise and decay, of the light curve.

3. The Landscape of Maser Flares

The variability index achievable by a particular flare mechanism varies considerably, from tens up to tens, or even hundreds, of millions. A strong controlling factor is the relative importance of supplying fresh inverted molecules to the system, and simple geometry. Models that rely on increasing the overall number density of inverted molecules over a significant proportion of a cloud tend to generate more powerful flares than those that are primarily geometric, and operate by increasing the column density of inverted molecules in selected directions. For example, variability of a radiative pump increases the inverted number density, as does the shock mechanism (which also selects for high column-density directions). Both of these can be very powerful; by contrast, rotors are purely geometric, and provide comparatively unspectacular flares. Line of sight overlaps also increase only the column density of inverted molecules at selected directions and velocities. The CVR mechanism appears, perhaps, not to fit this pattern, but it effectively provides a continuingly increasing number of inverted molecules from a velocity range that would normally be inaccessible, producing secondary gain in the maser (Field *et al.* 1994) until the catastrophe point is reached in velocity separation between the centres of the radiation line and molecular response. The variable background mechanism is an outlier in terms of the shape of the flare light curves it produces. It does change the number density of inverted molecules, but does so solely through saturation.

Given the variety of mechanisms considered in Section 1.1 to Section 1.6 above, we have attempted to use the different characteristic light curve shapes, timescales and variability indices to construct a diagnostic chart for deducing the underlying mechanism of each maser flare from a small number of observational parameters. Initially, we consider a plot of variability index against timescale for the mechanisms where periodicity is unlikely, in Figure 4, noting that the IR pump and background mechanisms that have been omitted for simplicity can appear anywhere on the plot to the right of the prohibited band, and

https://doi.org/10.1017/S1743921323002399 Published online by Cambridge University Press

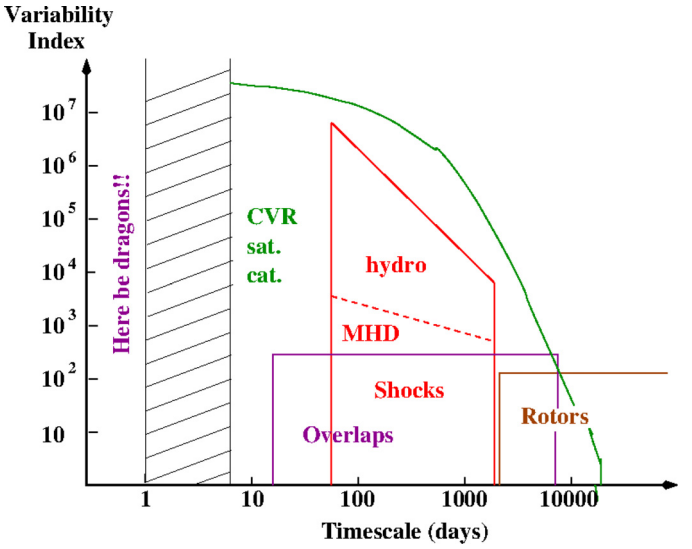

Figure 4. Zones in the variability index / timescale plane accessible to the shock, CVR, overlap and rotor mechanisms. The shaded region marks an approximate boundary between timescales accessible to the current model, and shorter times that would require a fully time-dependent model of the maser with simultaneous coupling to the gas dynamics.

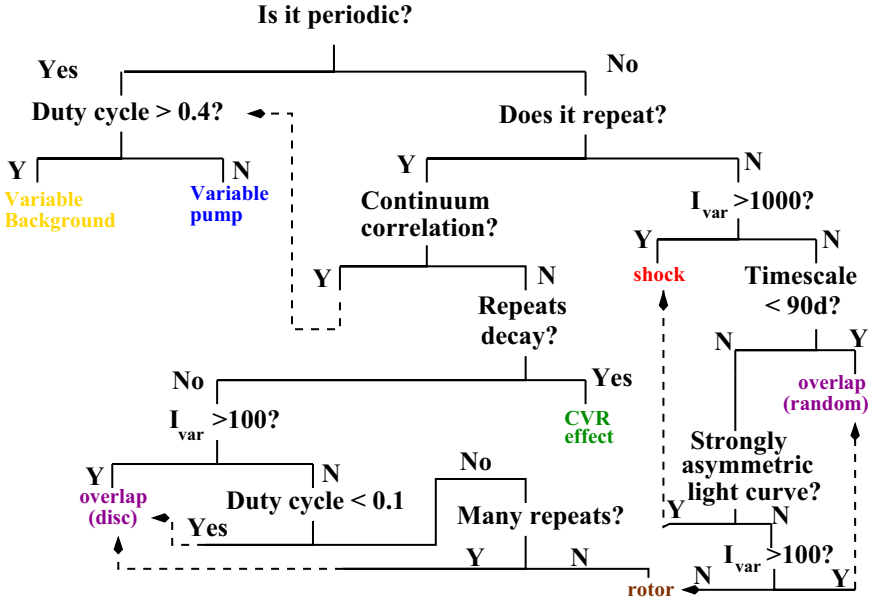

Figure 5. Our first attempt at a chart designed to identify the cause of a maser flare from observational properties of the light curve. The most fundamental choice is between periodic and non-periodic flares.

with suitable variability indices. Timescales for these two mechanisms are controlled by the driving functions.

With the loci of each mechanism in Figure 4 in mind, and an initial division into periodic and non-periodic sources, we have devised the diagnostic chart in Figure 5 that utilizes variability index (I_{var}) values, timescales and certain special features of light

https://doi.org/10.1017/S1743921323002399 Published online by Cambridge University Press

curves, such as the duty cycle for periodic sources, in order to derive flare mechanisms from observational parameters.

4. Conclusions

Details of the shape of the rise and decay in the light curve of a maser flare provide useful diagnostics of the flare mechanism. In many cases, a small number of parameters, the variability index, maximum observed flux density, and a temporal parameter, are sufficient to identify the mechanism responsible. The most powerful flares are generated by mechanisms that change the number density of the maser molecule in addition to geometrically increasing the column density along certain lines of sight, and optimum conditions include a maser that is unsaturated in the quiescent state, but becomes saturated during the flare.

Accurate analysis depends crucially on the availabiliy of high-cadence, multi-transition monitoring, as provided by the M2O organization, and also on the availability of contemporaneous continuum data in the radio and IR wavebands; the *NEOWISE* satellite mission (Nugent *et al.* 2015) deserves particular mention in this respect.

References

Bhardwaj, A., Kanbur, S. M., Marconi, M., Rejkuba, M., *et al.* 2017, *MNRAS*, 466, 2805
Burns, R. A., Kobak, A., Garatti o Caratti, A., *et al.* & Maser Monitoring Organization (M2O) 2022, European VLBI Network Mini-Symposium and Users' Meeting 2021, 12–14 July, 2021, 19
Cesaroni, R. 1990, *A&A*, 233, 513
Clegg, A. W. & Cordes, J. M. 1991, *ApJ*, 374, 150
Field, D., Gray, M. D., & de St. Paer, P. 1994, *A&A*, 282, 213
Goedhart, S., Gaylard, M. J., & van der Walt, D. J. 2004, *MNRAS*, 355, 553
Goedhart, S., Langa, M. C., Gaylard, M. J., & van der Walt, D. J. 2009, *MNRAS*, 398, 995
Goldreich, P. & Kwan, J. 1974, *ApJ*, 190, 27
Gray, M. D., Baggott, J., Westlake, J., & Etoka, S. 2019, *MNRAS*, 486, 4216
Gray, M. D., Etoka, S., & Pimpanuwat, B. 2020a, *MNRAS*, 498, L11
Gray, M. D., Etoka, S., Travis, A., & Pimpanuwat, B. 2020b, *MNRAS*, 493, 2472
Inayoshi, K., Sugiyama, K., Hosokawa, T., Motogi, K., & Tanaka, K. E. I. 2013, *ApJ*, 769, L20
Kaufman, M. J. & Neufeld, D. A. 1996, *ApJ*, 456, 250
Kobak, A., Bartkiewicz, A., Szymczak, M., *et al.* 2023, *A&A*, 671, A135
MacLeod, G. C., Smits, D. P., Goedhart, S., Hunter, T. R., *et al.* 2018, *MNRAS*, 478, 1077
Moscadelli, L., Sanna, A., Goddi, C., Walmsley, M. C., *et al.* 2017, *A&A*, 600, L8
Nugent, C. R., Mainzer, A., Masiero, J., Bauer, J., *et al.* 2015, *ApJ*, 814, 117
Olech, M., Szymczak, M., Wolak, P., Gérard, E., & Bartkiewicz, A 2020, *A&A*, 634, A41
Parfenov, S. Y. & Sobolev, A. M. 2014, *MNRAS*, 444, 620
Rajabi, F., Houde, M., Bartkiewicz, A., Olech, M., Szymczak, M., & Wolak, P. 2019, *MNRAS*, 484, 1590
Sobolev, A. M. 1993, Astrophysical Masers: Proceedings of the Conference, Arlington, VA, March 9–11, 1992, 219
Stecklum, B., Caratti o Garatti, A., Hodapp, K., Linz, H., Moscadelli, L., & Sanna, A. 2018, Astrophysical Masers: Unlocking the Mysteries of the Universe, volume 336 of IAU Symposium, 37
Sugiyama, K., Nagase, K., Yonekura, Y., Momose, M., *et al.* 2017, *PASJ*, 69, 59
Tanabe, Y., Yonekura, Y., & MacLeod, G. C. 2023, *PASJ*, 75, 351
van der Walt, D. J., Goedhart, S., & Gaylard, M. J. 2009, *MNRAS*, 398, 961
van der Walt, D. J., Maswanganye, J. P., Etoka, S., Goedhart, S., & van den Heever, S. P. 2016, *A&A*, 588, A47
Watson, W. D. & Wyld, H. W. 2000, *ApJ*, 530, 207

https://doi.org/10.1017/S1743921323002399 Published online by Cambridge University Press